Detection of acoustic pressure with hollow-core photonic bandgap fiber

Meng Pang and Wei Jin[*]

Department of Electrical Engineering, Hong Kong Polytechnic University, Hong Kong, China
[*]*Corresponding author: eewjin@polyu.edu.hk*

Abstract: We report the results of our preliminary investigation on the use of hollow-core photonic bandgap fiber (HC-PBF) for hydrophone application. The response of the commercial HC-1550-02 fiber to acoustic pressure, in terms of normalized responsivity (*NR*), is measured to be -334.4dB re $1\mu Pa^{-1}$. This agrees well with the theoretically predicated value of -331.6dB re $1\mu Pa^{-1}$ and is about 15dB higher than that of the conventional fiber (HNSM-155). With straightforward fiber structure modifications (thinner outer silica cladding and higher air-filling ratio of inner microstructured cladding), the *NR* could be further enhanced to -310dB re $1\mu Pa^{-1}$

©2009 Optical Society of America

OCIS codes: (060.2370) Fiber optics sensors; (120,5050) Phase measurement; (120.5475) Pressure measurement ; (060.5295) Photonic crystal fibers

References and links

1.   J. H. Cole, R. L. Johnson and P. G. Bhuta, "Fiber Optic Detection of Sound," J. Acoust. Soc. Am. **62**, 1136-1138 (1977).
2.   J. A. Bucaro, H. D. Dardy and E. F. Carome, "Fiber Optic Hydrophone," J. Acoust. Soc. Am. **62**, 1302-1304 (1977).
3.   C. K. Kirkendall and A. Dandridge, "Overview of high performance fiber-optic sensing," J. Phys. D **37,** 197-216 (2004).
4.   J. H. Cole et al, "Preliminary investigation of air-included polymer coatings for enhanced sensitivity of fiber-optic acoustic sensors," 15th Optical Fiber Sensors Conference (2002).
5.   G. B. Hocker, "Fiber optic acoustic sensors with composite structure: an analysis," Appl. Opt. **18**, 3679-3683 (1979).
6.   N. Lagakos, E. U. Schnaus, J. H. Cole, J. Jarzynski, and J. A. Bucaro, "Optimizing fiber coatings for interferometric acoustic sensors," IEEE J. Quantum Electron. **18**, 683-689 (1982).
7.   R. Hughes and J. Jarzynski, "Static pressure sensitivity amplification in interferometric fiber-optic hydrophones," Appl. Opt. **19**, 98-107 (1980).
8.   Crystal Fiber website, http://www.crystal-fibre.com
9.   B. Budiansky, D. C. Drucker, G. S. Kino, and J. R. Rice, "Pressure sensitivity of a clad optical fiber," Appl. Opt. **18**, 4085-4088 (1979).
10. L. J. Gibson and M. F. Ashby, *Cellular Solids: Structure and Properties*, *second edition*, (Cambridge University Press, New York 1997).
11. V. Dangui, H. K. Kim, Michel J. F. Digonnet, and Gordon S. Kino, "Phase sensitivity to temperature of the fundamental mode in air-guiding photonic-bandgap fibers," Opt. Express, 13, 6669-6684 (2005).
12. R. M. Christensen, "Mechanics of cellular and other low-density materials," Int. J. of Solids and Struct. 37, 93-104 (2000).
13. S. P. Timoshenko and J. Goodier, Theory of Elasticity (McGraw-Hill, New York, 1970).
14. J. H. Cole, S. Mothley, J. Jarzynski, A. B. Tveten, Clay Kirkendall, and Anthony Dandridge, "Air-Included Polymer Coatings for Enhanced Sensitivity of Fiber-Optic Acoustic Sensors," 16th Optical Fiber Sensors Conference, 214-217 (2003).
15. N. Lagakos, J. H. Cole, and J. A. Bucaro, "Acoustic sensitivity of fiber-optic interferometric sensors," Optical Fiber Communication Conference, ThGG3, 72-74 (1982).

16. Dandridge A, Tveten A B and Giallorenzi T G, "Homodyne demodulation scheme for fiber optic sensors using phase generated carrier," IEEE J. Quantum Electron. 18, 1647-53 (1982)

1. Introduction

Acoustic sensors based on the interferometric detection of pressure-induced phase shift of light propagating inside an optical fiber can be dated back to over 30 years ago [1, 2]. The phase accumulated by the fundamental mode through a fiber length L is given by

$$\phi = \frac{2\pi}{\lambda} n_{eff} L \tag{1}$$

where n_{eff} is the effective refractive index of the mode, and λ is the wavelength of light signal in vacuum. As acoustic pressure changes, both the fiber length L and the mode index n_{eff} (affected by the fiber transverse dimensions and the refractive indices of the materials forming the fiber) change, which result in a change in the signal phase. The acoustic sensitivity for nominal lengths of fiber in terms of normalized responsivity (NR) is expressed as [3]

$$NR = \frac{1}{\phi} \frac{d\phi}{dP} = \frac{1}{L} \frac{dL}{dP} + \frac{1}{n_{eff}} \frac{dn_{eff}}{dP} \tag{2}$$

where "dP" is the dynamic pressure acted on the fiber and "$d\varphi$" is the change in phase due to acoustic pressure. The two terms on the far right hand side of Eq. (2) corresponds respectively to acoustically-induced changes in the fiber length (the strain term) and in the refractive index (the index term).

Conventional bare silica fibers have relative low NRs, because of two reasons. Firstly, silica glass material has relative high Young's modulus, which makes the conventional fiber incompressible. By coating the silica fiber with a material with a lower Young's modulus, the effective Young's modulus of coated fiber can be reduced, and the fiber axial strain due to acoustic pressure (the strain term) can be increased [4, 5, 6 and 7]. Secondly, the refractive index change resulted from fiber strain, i.e., the index term, has opposite sign with respective to the strain term and hence compromises the NR .This undesirable "negative" index effect is anticipated to be greatly reduced in a HC-PBF in which most of the mode energy is confined in air. Since the current commercial HC-PBFs have similar coating materials and outer diameters as compared to conventional fibers [8], the NR of the HC-PBF is expected to be better. Furthermore, the flexibility offered by the stack-and-draw process, typically used for HC-PBF manufacturing, would allow HC-PBFs with larger area of holey microstructured region and smaller area of solid cladding region to be manufactured; this would further reduces the effective Young's modulus of the fiber and enhances the NR of the HC-PBF.
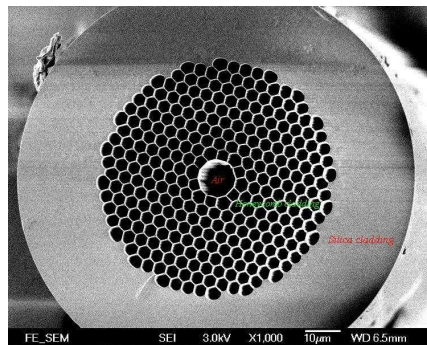

Fig. 1. SEM photograph of HC-PBF (HC-1550-02)

In this paper, we model the NR of HC-PBF with varying structural parameters and to compare the theoretical results with experimental results for a commercial HC-PBF (HC-1550-02), whose SEM photograph of cross-section is shown as Fig. 1. The experimental results agree well with the theory, which allows us to confidently use the model to predict the NR of HC-PBF with different structural parameters.

2. Theoretical Modeling

2.1 Elasticity model of HC-PBF

The model for computing the acoustic sensitivity of conventional bare and coated silica fibers were well described by Hocker, Lagakos and Budiansky [5, 6 and 9]. Unlike conventional silica fibers, a HC-PBF has an air-core instead of a silica core, an air-silica microstructured inner cladding with high air-filling ratio, a solid silica outer cladding, and an acrylete or other polymer jacket. The HC-PBF may be modeled as a structure with four circular regions: region 0 is the air core with radius of a; region 1 is the honeycomb inner cladding with thickness of b-a; region 2 is the silica outer cladding with thickness of c-b; and finally they are coated with the jacket region to the radius of d. The cross-section of the HC-PBF model is shown in Fig. 2.
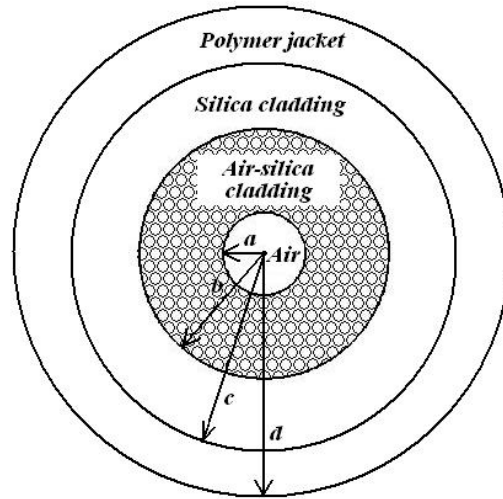

Fig. 2. Cross-section of a HC-PBF with an air core, a honeycomb air-silica inner cladding, a solid silica outer cladding and a polymer jacket.

Each layer is characterized by a certain elastic modulus E and Poisson's ratio v. The materials of silica outer cladding and jacket regions are homogeneous, and their Young's modulus and Poisson's ratios are E_2, E_3, and v_2, v_3 respectively. The honeycomb cladding of the HC-PBF is an exception in that it is not a homogeneous material but it behaves mechanically like a honeycomb [10, 11 and 12]. The Young's modulus and Poisson's ratio of a honeycomb are thus functions of air-filling ratio η. For a hexagonal pattern of air holes in silica, they are given by [10]:

$$\begin{cases} E_r = E_\theta = \dfrac{3}{2}(1-\eta)^3 E_0 = E_1^* \\ E_z = (1-\eta)E_0 = E_1 \end{cases} \qquad \begin{cases} v_{r-\theta} = v_{\theta-r} = 1 \\ v_{z-\theta} = v_{z-r} = v_0 \\ v_{r-z} = v_{\theta-z} \approx 0 \end{cases} \qquad (3)$$

Where E_0 is the Young' modulus of the silica material, v_0 is its Poisson's ratio, E_r, E_θ, E_z are the Young's modulus of the silica-air honeycomb in the three directions, and $v_{r\text{-}\theta}$, $v_{\theta\text{-}r}$, $v_{z\text{-}\theta}$, $v_{\theta\text{-}z}$, $v_{r\text{-}z}$, and $v_{z\text{-}r}$ are the six Poisson's ratio items of the honeycomb.

The stress expressions of the three regions may be expressed as [13]:

$$\begin{cases} \sigma_r^i = \dfrac{A_i}{r^2} + 2C_i \\[2mm] \sigma_\theta^i = -\dfrac{A_i}{r^2} + 2C_i \\[2mm] \sigma_z^i = D_i \end{cases}, \tag{4}$$

where A_i, C_i, and D_i (i-1,2,3) are constants. Using Hooke's law, we obtain the strain tensors of different layers shown as:

$$\begin{cases} \varepsilon_r^1 = \dfrac{2A_1}{E_1^* r^2} - v_1 \dfrac{D_1}{E_1} \\[2mm] \varepsilon_\theta^1 = -\dfrac{2A_1}{E_1^* r^2} - v_1 \dfrac{D_1}{E_1} \\[2mm] \varepsilon_z^1 = \dfrac{D_1}{E_1} \end{cases} \qquad \begin{cases} \varepsilon_r^i = \dfrac{1}{E_i}[(1+v_i)\dfrac{A_i}{r^2} + 2(1-v_i)C_i - v_i D_i] \\[2mm] \varepsilon_\theta^i = \dfrac{1}{E_i}[-(1+v_i)\dfrac{A_i}{r^2} + 2(1-v_i)C_i - v_i D_i] \qquad (i=2,3) \\[2mm] \varepsilon_z^i = \dfrac{1}{E_i}(D_i - 4v_i C_i) \end{cases} \tag{5}$$

There are nine constants to be determined: A_i, C_i, D_i ($i=1$, 2 and 3). According to the hydrostatic model [7], the boundary conditions of HC-PBF can be written as:

$$\sigma_r^1\big|_{r=b} = \sigma_r^2\big|_{r=b} \tag{a}$$

$$\sigma_r^2\big|_{r=c} = \sigma_r^3\big|_{r=c} \tag{b}$$

$$u_r^1\big|_{r=b} = u_r^2\big|_{r=b} \tag{c}$$

$$u_r^2\big|_{r=c} = u_r^3\big|_{r=c} \tag{d}$$

$$\sigma_r^1\big|_{r=a} = 0 \tag{e}$$

$$\sigma_r^3\big|_{r=d} = -(dP) \tag{f}$$

$$\varepsilon_z^1 = \varepsilon_z^2 = \varepsilon_z^3 \tag{g}$$

$$-(dP)d^2 = \sigma_z^1(b^2 - a^2) + \sigma_z^2(c^2 - b^2) + \sigma_z^3(d^2 - c^2) \tag{h}$$

(6)

where u_r^i is the radial displacement in the region i, which is related to strain by Eq. (7). Equations (6a) and (6b) describe radial stress continuity across the boundaries of regions, Eq. (6c) and Eq. (6d) describe the radial displacement continuity across the boundaries of the regions, Eq. (6e) means the fiber core is hollow, Eqs. (6f) and (6h) assume that the applied pressure is hydrostatic, and Eq. (6g) is for the plane approximation [14], which ignores end effects.

$$u_r^i = \int \varepsilon_r^i dr \tag{7}$$

Substituting Eqs. (4), (5) and (7) to the boundary conditions, the constants A_i, C_i, and D_i can be determined, and then the axial stress ε_z^1 of HC-PBF can be obtained. Considering the factor that the fundamental mode travels mostly in air, the changing of the fiber effective index caused by strains may be neglected [11]. The NR of HC-PBF depends mostly on the fiber axial stress and may be expressed as:

$$NR = \frac{(d\phi)}{\phi(dP)} \approx \frac{1}{L}\frac{dL}{dP} = \frac{\varepsilon_z^1}{dP} = \frac{D_1}{E_1 dP} \tag{8}$$

2.2 Predictions from the model

The physical parameters of a conventional fiber and a HC-PBF and the computed NR in dB (20Log(NR)) are listed in the Table 1. The theoretical NR of HC-PBF (HC-1550-02) manufactured by Crystal Fiber [8] was obtained from the model in Section 2.1. The NR of conventional silica fiber (HNSM-155) was computed by using the model described in Ref. [6].

Table 1. Physical parameters and predicted NRs of the solid and hollow-core fibers

	Conventional fiber (HNSM-155)	HC-PBF (HC-1550-02)
Region 0	--	Air a=5.45µm
Region 1	Silica Outer radius: 62.5µm Yong's modulus: 72GPa, Poission's ratio: 0.17	Honeycomb cladding b=35µm E_1=72GPa, v_1=0.17 η≈90%
Region 2	Acrylics Outer radius: 95µm Yong's modulus: 0.75GPa Poission's ratio: 0.45	Silica c=60µm E_2=72GPa v_2=0.17
Region 3		Acrylate d=110µm E_3=0.5GPa, v_3=0.37
NRs Predicted (dB re 1µPa^{-1})	-348.5	-331.6

From Table 1, the predicted NR of HC-1550-02 is about 15dB higher than the HNMS-155 fiber. This enhancement is mainly due to the reduction in mode index variation caused by fiber strain, which compromises the phase responsivity in conventional silica fibers.
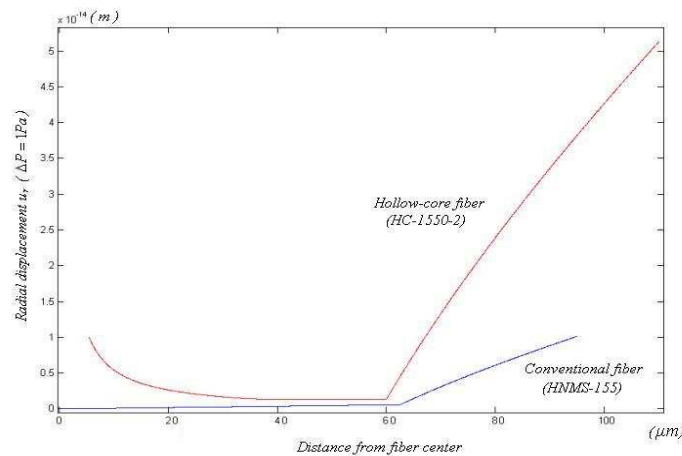

Fig. 3. Radial deformations as functions of distance from fiber center for the conventional fiber and HC-PBF. The core region (i.e., r< a=5.45µm) is hollow and the radial displacement is zero.

To further understand the predictions from the models, we plotted the radial displacements u_r as functions of distance from the fiber center for both the conventional fiber and the HC-PBF in Fig. 3. The reason for plotting the radial rather than the axial displacement is that the axial strain or displacement is the same everywhere under the plane approximation as given in Eq. (6g). The radial displacement distribution, although it is not directly related to the axial strain, reflect the relative rigidity of different regions, and the region with higher radial displacement is more flexible or compressible than the one with a lower radial displacement. Under the plane approximation, all the regions work in a coordinated manner to produce a single axial strain value (ε_z), and it is not difficult to image that a fiber with larger areas of compressible layers or regions would result in a larger axial strain and hence a larger NR as shown in Eq. (8). We observe that: first, in the conventional fiber over the silica region ($0 < r < 62.5\mu m$) the radial displacement remains small compared to the outer polymer coating region ($62.5\mu m < r < 95\mu m$). This is consistent with the Young's modulus and Poisson's ratio of the silica and polymer materials. It is high Young's modulus of silica (core and cladding) that limits the axial strain value of the conventional fiber, and hence the NR value. Second, in the HC-PBF, the radial displacement of the silica outer cladding ($35\mu m < r < 60\mu m$) remains small compared to the microstructured inner cladding and jacket regions, which indicates that the microstructured cladding and the polymer jacket are more compressible than the silica outer cladding. This again is consistent with mechanical properties (Young's modulus and Poisson's ratio) of the different layers. The rigid silica cladding constrains the deformation of the microstructured cladding and the polymer jacket, resulting in smaller radial displacements near the silica region. For the HC-PBF, it is the rigid silica outer cladding that limits the fiber's axial strain (ε_z) and hence the NR as shown in Eq. (8). Therefore it may be concluded that the thickness of the silica cladding layer is a main factor limiting the NR value of the HC-PBF, and the NR may be enhanced by reducing the thickness of this layer.

2.3 Design of HC-PBFs with enhanced NR

Based on the discussion in the Section 2.2, the thickness of the silica outer cladding is the main factor that limits the axial strain of the HC-PBF. Consequently, a thinner silica cladding layer is expected to result in a higher NR, and the highest value of NR would be achieved when the thickness of this layer is approaching zero. Since in the HC-PBF the fundamental mode travels mostly in air, the thickness of this silica cladding layer will make no effect to the optical properties of the HC-PBF.

These predictions were confirmed by numerical simulation by varying thickness of silica cladding region. In the simulation, only the value of *(c-b)* and the air filling ratio of honeycomb were varied, other parameters are the same as the HC-1550-02 fiber. Figure 4 shows the dependence of fibers' acoustic NRs on the thickness of the silica cladding. As expected, while the thickness of the silica cladding region is reduced (i.e., *c-b* decreases), NR increases. For higher air-filling ratios, NR is larger. The reason is that the honeycomb contains lesser silica at higher air-filling ratio, which results in a lower effective axial Young's modulus of fiber and thus higher axial strain due to acoustic pressure. When the silica layer thickness approaches zero, i.e. c→b→35µm, NR reaches its highest value of about -310dB for air-filling ratio of 97%. This is about 20dB higher than existing HC-1550-02 fiber, and more than 35dB higher than the conventional silica fiber.
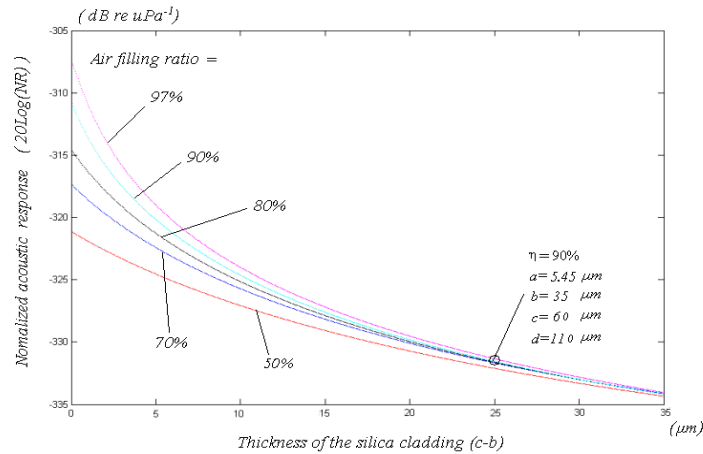
(dB re uPa⁻¹)

Fig. 4. NR of HC-PBF as functions of the thickness of the silica cladding *(c-b)* for different air filling ratios. Other parameters are fixed to *a*=5.45µm, *b*=35µm, and *d*=110µm. This graph is equivalent to c varying from 35 to 70µm.

3. Experiment and results

The acoustic NRs of the conventional silica fiber (HNSM-155 fiber from Fasten Fiberoptics) and the HC-PBF (HC-1550-02 from Crystal Fiber) were measured experimentally. The HC-1550-02 PBF is a single mode fiber at 1550nm with a effective mode index of ~0.99 and a attenuation of <0.03dB/m. Measurements were carried out using a Michelson fiber interferometer made from conventional single mode fibers with Faraday rotation mirrors (FRM) employed at the distal ends of both the sensing fiber and reference fiber to avoid polarization induced signal fading. The interferometer was illuminated with a fiber laser with the center wavelength of 1550nm and the line width of 10 kHz. The HC-1550-02 fiber was incorporated into the sensing arm of the interferometer, with one end spliced to one part of the 3-dB coupler and the other end to the pigtail of the FRM, as shown in Fig. 5.
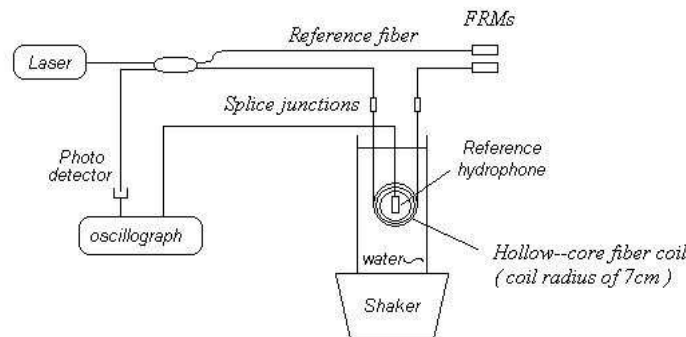

Fig. 5. Experimental setup

A standard hydrophone test tank was used to provide a low-frequency (40~1000Hz) test environment. Due to calibrator geometry, the fiber was coiled to a radius of 7cm to fit within the calibrator acoustic field. The radius of fiber coil is 7cm. A standard piezoelectrical hydrophone with the acoustic sensitivity (S_r) of -178 dB re v/µPa in the range of 10Hz~10000Hz was used as a reference to calibrate the fiber-optic hydrophone.

For sensitivity measurement at a particular acoustic frequency, the applied acoustic pressure was increased until the induced peak-peak phase shift of the interferometer reached 2π, a value easily determined from waveform displaced in the oscilloscope. When the response of the interferometer reached 2π, the values of the standard reference hydrophone outputs (V_r) were recorded. Figure 6 shows the typical result obtained from a sensing HC-1550-02 fiber of ~5.7m at the acoustic frequency of 500Hz. The upper trace is output from the photo-detector. The trace is a typical phase-modulation output of fiber interferometer [16], whose peak-peak phase change is 2π. The lower trace is response of standard hydrophone to the acoustic field.
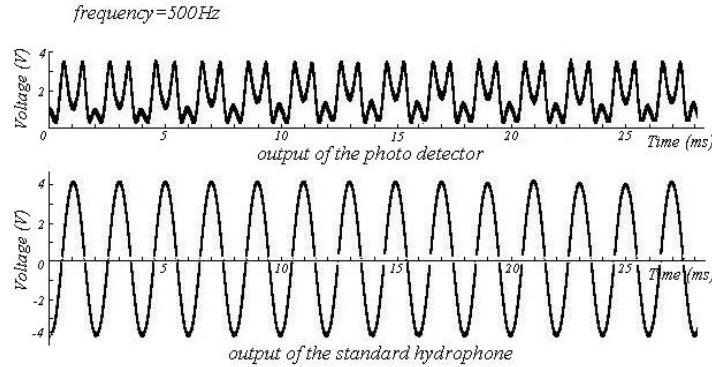

Fig. 6. A typical experimental result (f=500Hz), the upper trace is the output from the fiber hydropone for a peak-peak phase change of 2π; the lower is the standard piezoelectrical hydrophone corresponds to the 2π phase change

The fiber's acoustic sensitivity (S) is then calculated as:

$$S = S_r + 20\log(2\pi / V_r) \tag{9}$$

Then, from Eqs. (1), (2) and (9) the acoustic NR of the fiber can thus be determined by:

$$NR = S - 20\log(\frac{2\pi n_{eff} L}{\lambda}) - 6 \tag{10}$$

The -6dB in Eq. (10) is because the measurement was taken with a Michelson interferometer, in which the light goes through the sensing fiber twice.

The experiment was repeated for different acoustic frequencies and the measured frequency response is shown in Fig. 7. For comparison, the frequency response of the HNSM-155 fiber was also measured with a similar experimental setup and shown in Fig.7. The average values of NR over 200Hz~1000Hz for the HC-1550-02 is -334.4dB re μPa^{-1}, 15dB higher than that of the HNSM-155 fiber. These experimental results agree well with the theoretical ones as summarized in Table. 2.
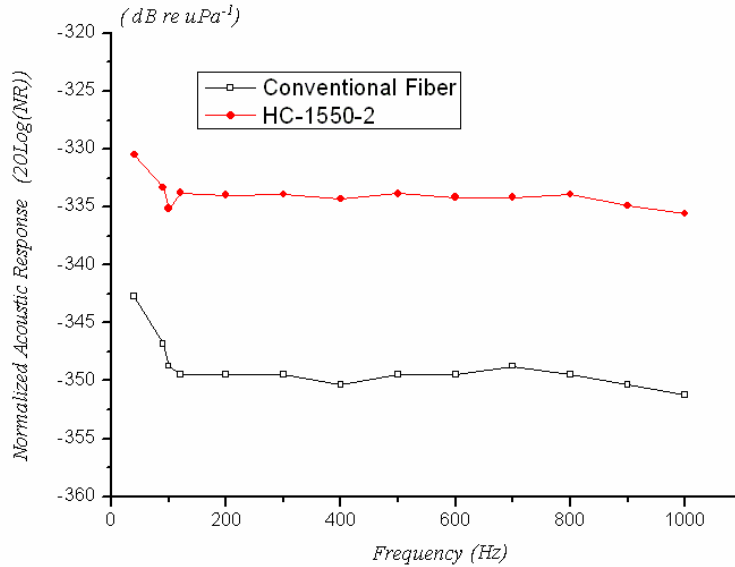
Fig. 7. Measured NR of conventional HNSM and HC-1550-02 fibers as functions of frequency

Table 2 Parameters, measured NRs and predicted NRs of conventional fiber and HC-PBF

	Conventional Fiber (HNSM-155)	HC-PBF (HC-1550-02)
Predicted NRs (dB re $1\mu Pa^{-1}$)	-348.5	-331.6
L (m)	9.5	5.7
n_{eff}	1.46	0.997
Measured NRs (dB re $1\mu Pa^{-1}$)	-349.4	-334.4

4. Conclusion

In conclusion, we have investigated theoretically and experimentally the acoustic sensitivity of air-silica HC-PBFs and compared with conventional silica single mode fiber hydrophones. Theoretical modeling shows that the main factor that affects the normalized acoustic response of the HC-PBF is the thickness of fiber's silica outer cladding layer and the air-filling ratio of the air-silica microstructured inner cladding. The NR of the commercial HC-1550-02 PBF was experimentally measured to be -334.4 dB re $1\mu Pa^{-1}$, and is about 15 dB higher than that of the conventional HNSM-155 fiber. These values agree well with the results of our theoretical modeling and give us the confidence to use our theoretical models to predict the performance of HC-PBF with varying structural parameters. By using a thin outer cladding of the order of a few micrometers or less and an air-filling ratio of 95% or higher, it is theoretically possible to enhance the NR of the HC-PBF to up to -310dB, about 35dB higher than conventional silica fibers. The reduction in the thickness of the HC-PBF's outer silica cladding would weaken the mechanical strength of the fiber, and this could be a issue when it is used under high static pressure environment such as in deep water. This is a topic of further investigation.

The NR could be further enhanced by using proper air-included polymer coating [4 and 14], which would significantly increase the NR of the HC-PBF and will be the subject of further study. The great enhancement of NR is anticipated to have important practical benefits for the simplification and cost reduction of multi-sensor arrays by avoiding the use of air-backed mandrels [3].

Acknowledgment